

## ESR MODES IN HEXAGONAL ABX<sub>3</sub>-TYPE ANTIFERROMAGNETS

H. Tanaka, S. Teraoka, E. Kakehashi, K. Iio and K. Nagata

*Department of Physics, Faculty of Science, Tokyo Institute of Technology, Oh-okayama, Meguro-ku, Tokyo 152, Japan*

**Abstract.** – ESR modes in the ground state of hexagonal ABX<sub>3</sub>-type antiferromagnets are discussed by taking a six-sublattice model for the spin structure. Results of ESR measurements performed on CsNiCl<sub>3</sub>, RbNiCl<sub>3</sub> and CsMnI<sub>3</sub> are reported. Calculated frequency-field diagram is in agreement with experimental one.

Hexagonal ABX<sub>3</sub>-type antiferromagnets such as CsNiCl<sub>3</sub>, RbNiCl<sub>3</sub>, CsCoCl<sub>3</sub> etc. are one of magnetic systems of special interest, because they are good approximations of a one-dimensional magnetic system and many of them undergo successive phase transitions owing to the spin frustration effect on the triangular lattice in the *c*-planes [1-3]. To date detailed experimental and theoretical work has been performed to clarify the magnetic properties of the present compounds [4-12]. There are some brief reports on the ESR measurements made at the low-temperature region [12]. However the resonance modes have not been understood even in the ground state. Recently we have made precise ESR measurements on the present compounds in the temperature range including the phase transition points [13]. In this note, we present the results of theoretical calculations on the ground state properties of the resonance modes, and compare the experimental results with the calculations.

The systems considered here correspond to substances whose B<sup>2+</sup> ion is Ni<sup>2+</sup>, Mn<sup>2+</sup> and V<sup>2+</sup>. For that case the Hamiltonian of the system is well described by the Heisenberg model with small uniaxial anisotropy with respect to the *c*-axis. Both the intrachain and interchain couplings (*J*<sub>0</sub> and *J*<sub>1</sub>) are taken to be antiferromagnetic. For easy-axis anisotropy case, spin moments in one-third of the chains are parallel to the *c*-axis and those in the rest of chains are canted from the *c*-axis. For easy-plane anisotropy case, spin moments form the 120°-structure in the *c*-planes. Since the intrachain coupling is antiferromagnetic in both the cases, the spin arrangement can be divided into six sublattices (*i* = 1 ~ 6). The free energy at sufficient low temperatures may be expressed as

$$F = - \sum_{i=1}^6 \mathbf{M}_i \cdot \mathbf{H} + A (\mathbf{M}_1 \cdot \mathbf{M}_4 + \mathbf{M}_2 \cdot \mathbf{M}_5 + \mathbf{M}_3 \cdot \mathbf{M}_6) + B (\mathbf{M}_1 \cdot \mathbf{M}_2 + \mathbf{M}_2 \cdot \mathbf{M}_3 + \mathbf{M}_3 \cdot \mathbf{M}_1 + \mathbf{M}_4 \cdot \mathbf{M}_5 + \mathbf{M}_5 \cdot \mathbf{M}_6 + \mathbf{M}_6 \cdot \mathbf{M}_4) + \frac{1}{2} K \sum_{i=1}^6 (M_i^z)^2, \quad (1)$$

where *M<sub>i</sub>* is the magnetization of the *i*-the sublattice,

*H* is an external field, *A* and *B* are intrachain and interchain coupling constants, respectively, and *K* is anisotropy constant (*A* ≫ *B*, |*K*|).

The normal modes for the motions of the sublattice magnetizations are obtained by the solutions of the set of equations,  $d\mathbf{M}_i / dt = \gamma [\mathbf{M}_i \times \mathbf{H}_i]$ , where *H<sub>i</sub>* is the mean field acting on the *i*-th sublattice and is given by  $\mathbf{H}_i = -(\partial F / \partial \mathbf{M}_i)$ . When *A* ≫ *B*, |*K*|, the above equations of motion can be analytically solved for  $\mathbf{H} // C$  and  $\mathbf{H} \perp C$ . Calculated frequency-field diagrams for the easy-axis (*K* > 0) and easy-plane (*K* < 0) anisotropy cases are shown in figure 1, where a condition *B* = 2 |*K*| is taken as an example. In the spin-flop phase for *K* > 0, the *c*-plane components of the spin moments form the 120°-structure, and for *K* < 0, the components of spin moments projected on the plane perpendicular to the external field form a triangular structure. In general six kinds of modes are obtained. The observable modes are such that the total magnetization is in motion (precession or oscillation).

For easy-axis anisotropy case, a gap-less ω<sub>1</sub>-mode given by ω / γ = *H* ( $\mathbf{H} \perp C$ ) attracts our attentions. In this mode, *M*<sub>1</sub> and *M*<sub>4</sub> corresponding to the spin moments parallel to the *c*-axis do not move. For *K* > 0, the interchain exchange interaction and the anisotropy compete with each other and the spin structure is determined on the balance of the both. This competition is responsible for the lack of the gap energy of the ω<sub>1</sub>-mode. This ω<sub>1</sub>-mode has actually been observed in CsNiCl<sub>3</sub>, RbNiCl<sub>3</sub>, CsNiBr<sub>3</sub>, RbNiBr<sub>3</sub> and CsMnI<sub>3</sub>, all of which have easy-axis anisotropy and form the triangular structure in the *ac*-planes in the low-temperature phase. The other notable mode for *K* > 0 is the ω<sub>5</sub>-mode whose gap energy lowers as the ratio *K* / *B* decreases. For  $\mathbf{H} // C$ , the ω<sub>5</sub>-mode shows softening and its frequency goes to zero at the transition field  $H_c = \sqrt{2AKM_0}$ , where *M*<sub>0</sub> is the magnitude of the sublattice magnetization.

Shown in figure 2 are experimental frequency-field diagrams for CsNiCl<sub>3</sub> and CsMnI<sub>3</sub>, where solid lines denote the theoretical curves calculated with parameters given in table I, where the anisotropy constant *K* and interchain exchange field constant *B* are estimated

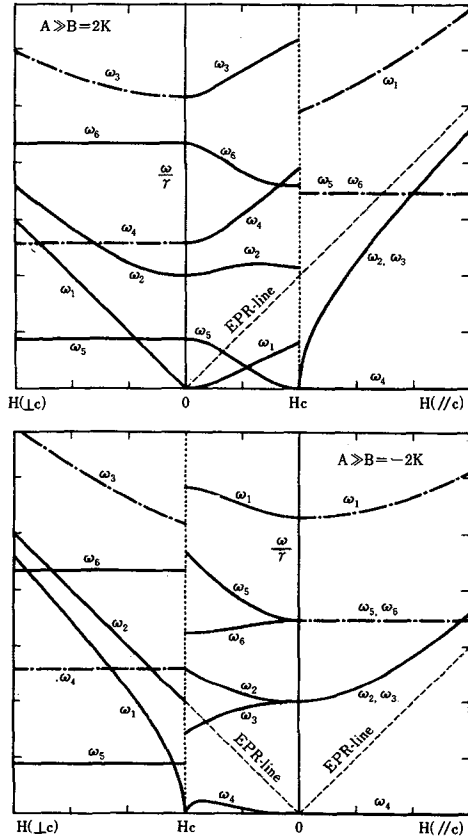


Fig. 1. - Frequency-field diagrams for (a) easy-axis ( $K > 0$ ) and (b) easy-plane ( $K < 0$ ) anisotropy cases. Solid and dot-dashed lines denote observable and unobservable modes, respectively.

Table I. - Magnetic parameters of  $\text{CsNiCl}_3$  and  $\text{CsMnI}_3$ , where  $\theta$  denotes an angle between the canted spin moments and the  $c$ -axis at  $H = 0$ .

	$\text{CsNiCl}_3$		$\text{CsMnI}_3$	
$AM_0$	380 kOe	[12]	680 kOe	[9]
$BM_0$	1.1 kOe		8.3 kOe	
$KM_0$	0.49 kOe		2.2 kOe	[9]
$H_c$	19.2 kOe	[12]	54 kOe	
$T_N$	$T_{N1} = 4.84$ K		$T_{N1} = 11.42$ K	[9]
	$T_{N2} = 4.40$ K	[2]	$T_{N2} = 8.20$ K	[11]
	$g_{\parallel} = 2.18(7)$		1.99	
	$g_{\perp} = 2.20(3)$		2.00	
	$\theta = 50.3^\circ$		$55.0^\circ$	

from the transition field  $H_c$  and the gap energy of the  $\omega_5$ -mode, respectively. Calculated values of fields for resonance are in agreement with the experimental results. For  $\text{RbNiCl}_3$ , the  $\omega_5$ -mode could not be observed in the frequency range higher than  $X$ -band. Therefore  $B$  may be fairly greater than  $K$  in  $\text{RbNiCl}_3$ . Details of the present study will be published elsewhere [13].

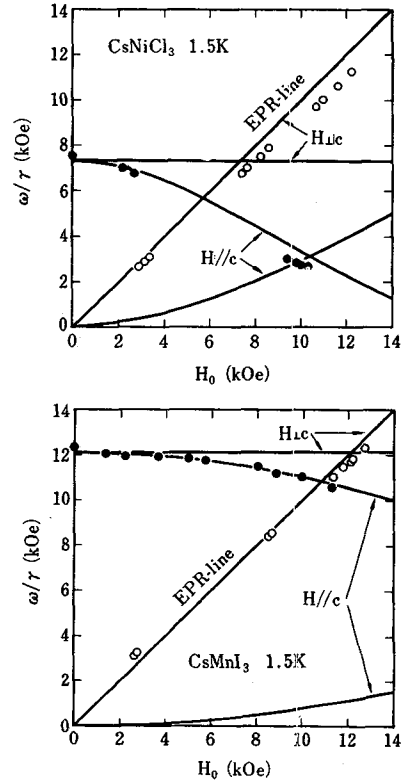


Fig. 2. - Experimental frequency-field diagrams for (a)  $\text{CsNiCl}_3$  and (b)  $\text{CsMnI}_3$ . Solid lines denote theoretical values.

- [1] Achiwa, N., *J. Phys. Soc. Jpn* **27** (1969) 561.
- [2] Clark, R. H. and Moulton, W. G., *Phys. Rev. B* **5** (1972) 788.
- [3] Brener, R., Ehrenfreund, E. and Shechter, H., *J. Phys. Chem. Solids* **38** (1977) 1023.
- [4] Mekata, M., *J. Phys. Soc. Jpn* **42** (1977) 76.
- [5] Matsubara, F., *J. Phys. Soc. Jpn* **51** (1982) 2424.
- [6] Plumer, M. L., Hood, K. and Ceillé, A., *Phys. Rev. Lett.* **60** (1988) 45.
- [7] Minkiewicz, V. J., Cox, D. E. and Shirane, G., *Solid State Commun.* **8** (1970) 1001.
- [8] Yelon, W. B. and Cox, D. E., *Phys. Rev. B* **6** (1972) 204; *Phys. Rev. B* **7** (1973) 2024.
- [9] Zandbergen, H. W., *Solid State Chem.* **35** (1980) 367.
- [10] Iio, K., Hyodo, H. and Nagata, K., *J. Phys. Soc. Jpn* **49** (1980) 1336.
- [11] Iio, K., Hotta, H., Sano, M., Masuda, H., Tanaka, H. and Nagata, H., *J. Phys. Soc. Jpn* **57** (1988) 50.
- [12] Cohen, E. and Sturge, M. D., *Solid State Commun.* **24** (1977) 51.
- [13] Tanaka, H., Teraoka, S., Kakehashi, E., Iio, K. and Nagata, K., *J. Phys. Soc. Jpn* **57** (1987) 3979.